Device-Free Localization: Outdoor 5G Experimentation at mm-Waves

Carlos A. Gómez-Vega, *Graduate Student Member, IEEE*, Oluwatayo Y. Kolawole, *Member, IEEE*, Mythri Hunukumbure, *Senior Member, IEEE*, Tomasz Mach, Moe Z. Win, *Fellow, IEEE*, and Andrea Conti, *Fellow, IEEE*

***Abstract*— Device-free localization (DFL) will enable several use cases of fifth generation (5G) and beyond 5G (B5G) ecosystems that rely on position information of non-collaborative targets. While current 5G systems support device-based localization, their sensing capabilities for providing DFL have not been unleashed. This letter presents an experimentation and measurement campaign for outdoor device-free target detection and localization using as transmitter a 5G fixed wireless access at millimeter waves (mm-Waves), namely in the 28 GHz band. Specifically, the experimentation focuses on exploring the sensing capabilities of 5G systems to determine the positions of device-free targets. Experimental results show the potential of 5G DFL at mm-Waves.**

***Index Terms*— Device-free localization, 5G, mm-Waves, angle estimation, experimentation.**

I. Introduction

LOCATION AWARENESS is crucial in 5G and B5G ecosystems [1], [2], [3], [4] to enable several applications and use cases, including intelligent transportation, public safety, and smart environments. Current 5G standardization supports localization of collaborative targets (e.g., people, vehicles, and objects) equipped with user equipments (UEs) or dedicated devices [1]. The integration of sensing capabilities in 5G ecosystems will enable use cases relying on position information of non-collaborative targets that do not exchange radio signals by means of a specific device [3], [5]. In particular, DFL requires sensing and processing the reflections caused by non-collaborative targets [6], [7], [8]. Accurate detection and localization of device-free targets using 5G systems is difficult since their sensing capabilities have not been unleashed.

In 5G ecosystems, DFL relies on measurements obtained by receivers that process signals emitted by 5G base stations (BSs) or UEs and reflected by targets. For example, 5G fixed wireless access (FWA) technology can provide ubiquitous emissions for DFL due to its widespread deployment [9]. Specifically, the receivers can be dedicated sensors or 5G nodes that collect direct signals from transmitters and signals reflected by both the background and the targets [2], [3]. Performance requirements for DFL in 5G ecosystems include localization accuracy, as well as misdetection and false alarm rates [3]. While 5G standardization specifies reference signals for device-based localization [1], 5G DFL can rely either on dedicated waveforms (i.e., reference signals for sensing) or communication signals already in the air (i.e., signals of opportunity in passive radar settings [10], [11], [12]). With the adoption of frequency bands at mm-Waves, i.e., the frequency range 2 (FR2) in 5G specifications [13], localization and sensing capabilities are enhanced due to the use of greater bandwidth and large antenna arrays [14], [15]. In particular, beamforming is a key enabler for communication at mm-Waves [16], [17], additionally allowing sensing in the angular space [18], [19], [20].

Initial efforts by the 3rd Generation Partnership Project (3GPP) on integrated sensing and communication (ISAC) in 5G ecosystems have focused on describing use cases and potential requirements to collect sensing information [3]. However, standardized sensing procedures for 5G ecosystems are still missing since their sensing capabilities, especially those exploiting existing functionalities, have not been explored. While the vision of B5G networks has motivated the design of new waveforms for ISAC [5], 5G systems offer the possibility of integrating DFL without modifying neither the standardized signaling nor the baseband processing. Coherent target detection using sub-6 GHz 5G signals has been demonstrated via experimentation with dedicated receivers [21], [22]. In addition, time-difference-of-arrival (TDOA) and angle-of-arrival (AOA) estimation for DFL using 5G mm-Wave signals has been studied via simulation [23]. Furthermore, extensive measurement campaigns have been performed to characterize wireless propagation at mm-Waves [24], [25], [26]. However, those experiments are not suitable for the characterization of DFL since they do not explicitly consider the reflections from device-free targets. Compared to 5G device-based localization [2], ISAC [5], and DFL via mm-Wave radar [27], research on 5G DFL at mm-Waves is limited.

The goal of this letter is to show the potential of 5G DFL at mm-Waves via experimentation. We believe that DFL at mm-Waves can be seamlessly integrated into 5G ecosystems by unleashing their sensing capabilities without modifying the standardized signaling and baseband processing. The key idea consists of exploiting beam sweeping procedures of 5G systems to obtain position information of device-free targets.

Manuscript received 4 April 2023; revised 17 May 2023; accepted 10 June 2023. Date of publication 26 June 2023; date of current version 12 September 2023. The fundamental research described in this letter was supported, in part, by the European Union's Horizon 2020 Research and Innovation Programme under Grants 871249 and 815279, by the Office of Naval Research under Grant N62909-22-1-2009, by the National Science Foundation under Grant CNS-2148251, and by funds from federal agency and industry partners in the RINGS program. The associate editor coordinating the review of this letter and approving it for publication was W. Yuan. *(Corresponding author: Andrea Conti.)*

Carlos A. Gómez-Vega and Andrea Conti are with the Department of Engineering and CNIT, University of Ferrara, 44122 Ferrara, Italy (e-mail: cgomez@ieee.org; a.conti@ieee.org).

Oluwatayo Y. Kolawole, Mythri Hunukumbure, and Tomasz Mach are with the Samsung Electronics Research and Development Institute U.K., TW18 4QE Staines, U.K. (e-mail: o.kolawole@samsung.com; mythri.h@samsung.com; tomasz.mach@samsung.com).

Moe Z. Win is with the Laboratory for Information and Decision Systems, Massachusetts Institute of Technology, Cambridge, MA 02139 USA (e-mail: moewin@mit.edu).

Digital Object Identifier 10.1109/LCOMM.2023.3289652

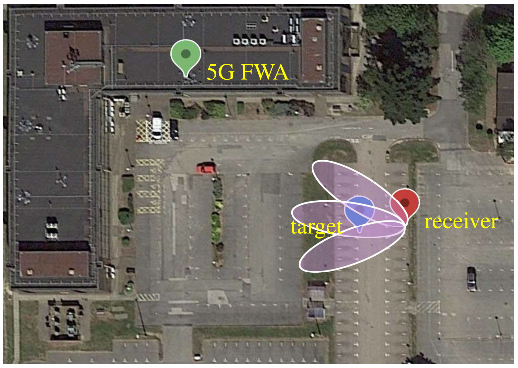

(a) Experimentation environment.

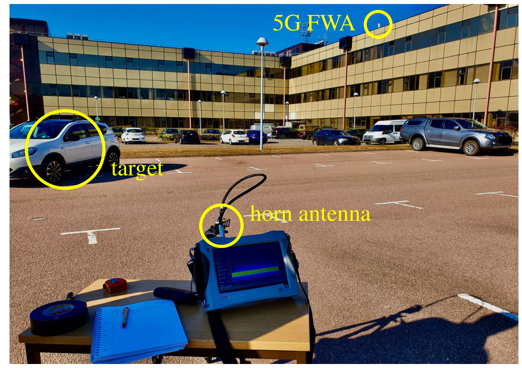

(b) Experimental setup.

Fig. 1. Views of: (a) experimentation environment with a pair of receiver and target positions; and (b) experimental setup with a vehicle as a static target (Map data: Google Earth©, 2023).

This letter presents an experimentation and measurement campaign for device-free target detection and localization using a 5G FWA at 28 GHz as transmitter in an outdoor parking lot. The experiments focus on exploring the sensing capabilities of 5G systems at mm-Waves to provide DFL. The key contributions of this letter can be summarized in the following.

- Exploration of 5G DFL at mm-Waves via experimentation in an outdoor environment.
- Quantification of 5G DFL performance via simulations based on models extracted from measured data.

The remaining sections are organized as follows: Section II describes the measurement campaign. Section III presents results on target detection. Section IV describes an angle estimation method compatible with the current 5G architecture and develops AOA measurement models. Section V presents the 5G DFL performance based on the experimentation. Finally, Section VI presents our final remark.[1]

II. Measurement Campaign

We present an experimentation that focuses on exploring the sensing capabilities of 5G systems to detect and locate device-free targets.[2] In particular, the transmitter is a BS and the receiver is a UE. In 3GPP specifications, the situation in which a UE serves as the sensing receiver processing the received signals and communicating the results to the 5G system is referred to as *transparent sensing* [3, Section 5.4]. We consider that the receiver employs beam sweeping procedures to sense the environment similar to those used for communication and device-based localization in 5G systems [17]. Specifically, coarse AOA estimates are obtained by identifying the direction of the beam with the highest received power [15]. Such estimates are used to steer the beam toward the direction that maximizes the signal-to-noise ratio and as measurements for position inference. This sensing operation is analogous to that employed in phased-array radar systems [6].

[1]*Notations*: Random variables are displayed in sans serif, upright fonts (e.g., x); their realizations in serif, italic fonts (e.g., x). Vectors are denoted by bold lowercase letters (e.g., $\boldsymbol{x}$). Sets are denoted by calligraphic fonts (e.g., $\mathcal{S}$).

[2]The 28 GHz radio measurements used in this letter were conducted by Samsung Research UK in the 5G VINNI test facility at BT Labs Ipswich, UK, with support from BT Labs.

The experimental setup consists of a 5G FWA operating at 28 GHz under 5G Technology Forum specifications [28] and a spectrum analyzer as transmitter and receiver, respectively, in a bistatic configuration. The experimentation environment is an outdoor parking lot located in front of an L-shaped building on top of which the 5G FWA is installed (see Fig. 1(a)). The 5G FWA emits a 5G probe signal with center frequency and bandwidth of 27.35 GHz and 100 MHz, respectively. The equivalent isotropically radiated power of the 5G FWA is 54 dBm. The spectrum analyzer measures the received power using a 30° horn antenna with directional gain of 15 dBi. The receiver is placed in different positions with the antenna steered to prescribed directions covering the 360° angular space. This experimentation approach reproduces practical beam sweeping procedures that rely on measurements of the received power [16], [17]. We consider the direction of the direct path as the reference direction for each receiver position. The direction of the direct path is determined by searching for the direction with the highest received power in line-of-sight (LOS) conditions. For each receiver position, we perform multiple experiments involving both static and mobile targets. The horizontal distance between the positions of the 5G FWA transmitter and the receiver ranges from 53.2 to 80.1 m. The horizontal distance between the receiver and static target positions ranges from 7.6 to 11.4 m. Fig. 1(b) shows the experimental setup with a vehicle as a static target. Note that the vehicle in the experimentation is an extended target due to its size and separation distance with the receiver.

For the analysis, we consider the frequency-averaged and time-averaged received power. Let $S_\theta(t,f)$ denote a realization of the received power spectral density in the direction θ at time $t \in [0, T_\mathrm{o}]$ and frequency $f \in [f_\mathrm{L}, f_\mathrm{U}]$, where T_o is the observation time, and f_L and f_U are the lower and upper frequencies of the measured bandwidth, respectively. The frequency-averaged received power at time t is given by

$$\gamma_\theta(t) = \int_{f_\mathrm{L}}^{f_\mathrm{U}} S_\theta(t,f)\, df. \tag{1}$$

The time-averaged received power at frequency f is given by

$$\varrho_\theta(f) = \int_{0}^{T_\mathrm{o}} S_\theta(t,f)\, dt. \tag{2}$$

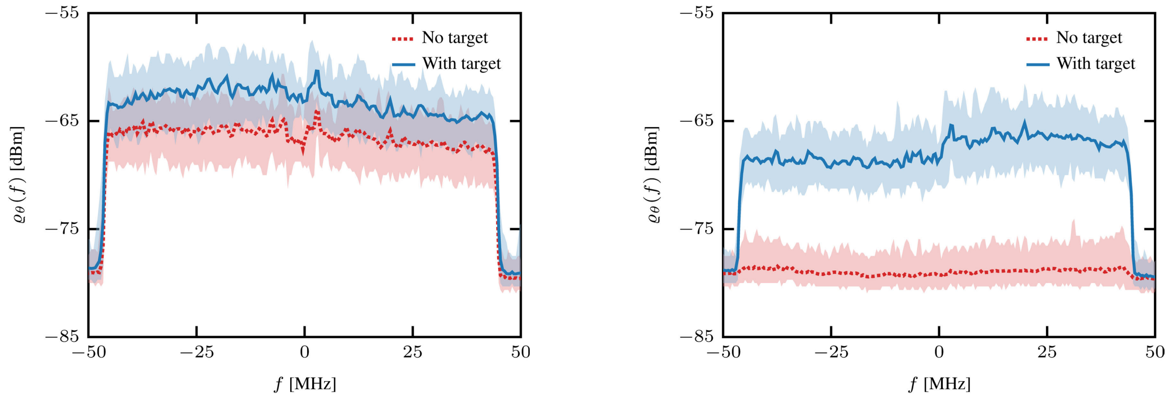

(a) Antenna steered 30° anticlockwise from reference direction.

(b) Antenna steered 60° anticlockwise from reference direction.

Fig. 2. Time-averaged received power of experiments with and without a static target and the antenna steered (a) 30° and (b) 60° anticlockwise from the reference direction. The shaded areas depict the range of the measured power in the corresponding experiments. In these experiments, the horizontal transmitter-to-receiver and receiver-to-target distances are 64.6 and 11.3 m, respectively. The center frequency corresponds to 27.35 GHz.

In addition, we consider measurements $P_\theta = \gamma_\theta(\check{t})$ in the direction θ sampled at generic times $\check{t}$.

III. Target Detection

This section presents experimental results regarding target detection, which is essential for DFL. The presence of static and mobile scatterers in the environment generates background clutter, i.e., undesired signal components that are not related to targets and affect their detection [8], [29]. In addition, the signal propagating via the direct path can leak into the received waveform and mask weak reflections from targets [6], [7].

Fig. 2 shows the time-averaged received power $\varrho_\theta(f)$ of experiments in a fixed receiver position with and without a static target and the antenna steered 30° and 60° anticlockwise from the reference direction. We consider a fixed target position for each receiver position and steer the receiving antenna in the presence and absence of the target. The receiver captures reflections related to the target in these directions due to its size and the beamwidth of the antenna. In these experiments, the receiver captures strong signal components from the direct path and clutter with the antenna steered 30° anticlockwise. In contrast, the receiver does not capture significant contributions from the direct path and clutter with the antenna steered 60° anticlockwise. Note that, in the presence of the target, the received power is higher compared to the case without it. The differences (in dB) between the received power in the experiments with the target and that of the experiments without the target are 3.3 and 10.7 dB when the antenna is steered 30° and 60° anticlockwise, respectively. These results indicate the feasibility of device-free target detection using 5G systems operating at mm-Waves by performing sensing through beam sweeping procedures, e.g., via non-coherent techniques based on thresholds for the received power level.

Next, we analyze how the propagation loss at mm-Waves can affect target detection by considering different distances between transmitter and receiver. Table I shows the sample mean of measurements P_θ in experiments with and without a static target for different distances between transmitter and receiver and various clutter conditions. The measurements with and without the target are denoted by superscripts (T) and (N), respectively. The table reports $P_\theta^{(\mathrm{T})}/P_\theta^{(\mathrm{N})}$ (in dB) for further comparison. The levels of clutter are classified based on empirical observations of the environment as Mild, Moderate, and Severe. Note that the received power increases in the presence of the target for all the experimental conditions. However, the gain obtained in the presence of the target decreases either as the distance increases or as the clutter conditions worsen. For example, the ratio $P_\theta^{(\mathrm{T})}/P_\theta^{(\mathrm{N})}$ decreases for the experiments in mild clutter conditions as the distance increases. This decrease with respect to the distance is due to the high propagation loss characteristic of mm-Wave channels [24], [25], [26]. The last experiment reported in Table I has a higher gain in the presence of the target due to a different position of the vehicle that is more favorable for reflecting the signal compared to the rest of the configurations.

TABLE I

Sample Mean of the Frequency-Averaged Received Power With and Without a Static Target in Different Conditions

Distance [m]	Clutter	$P_\theta^{(\mathrm{T})}$ [dBm]	$P_\theta^{(\mathrm{N})}$ [dBm]	$P_\theta^{(\mathrm{T})}/P_\theta^{(\mathrm{N})}$ [dB]
57.3	Mild	−68.23	−78.96	10.73
57.3	Severe	−63.70	−67.01	3.31
64.6	Moderate	−68.65	−74.19	5.54
68.5	Mild	−67.92	−78.33	10.41
72.5	Mild	−72.91	−77.91	5.00
75.6	Mild	−73.64	−76.00	2.36
80.1	Mild	−64.45	−78.70	14.25

Consider experiments for a mobile target on a linear trajectory of 12 m with a speed of 5 km/h. Fig. 3 shows the frequency-averaged received power $\gamma_\theta(t)$ of experiments in a fixed receiver position with the mobile target and the antenna steered 45° and 60° anticlockwise from the reference direction. It can be observed that the target enters into and exits from the field of view of the considered beams. In particular, the target can be detected by overlapping beams at the same time instant (cf. Fig. 2 for the static target case) due to the increase in the received power when it is within the area covered by the beam. While the direction of the beam detecting the target provides a coarse angle estimate, the information from multiple beams detecting it can be used to improve the accuracy.

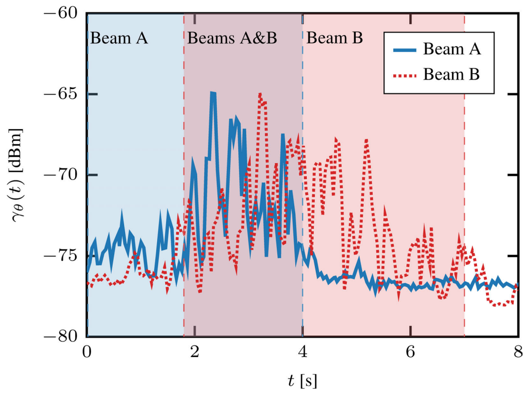

Fig. 3. Frequency-averaged received power of experiments with a mobile target and the antenna steered 45° (beam A) and 60° (beam B) anticlockwise from the reference direction. The shaded areas depict the time windows in which the target can be detected by the beams indicated. In these experiments, the horizontal transmitter-to-receiver distance is 68.5 m.

IV. AOA Estimation and Measurement Models

This section describes an angle estimation method compatible with the current 5G architecture and develops AOA measurement models to explore 5G DFL at mm-Waves.

A. AOA Estimation

Consider a receiver sensing a wireless environment via beam sweeping (see Fig. 1(a)). The receiver scans the environment by steering N_b beams with index set $\mathcal{N}_\mathrm{b} = \{1, 2, \dots, N_\mathrm{b}\}$ and detects a target in N_d adjacent and partially overlapping beam patterns with indices $\mathcal{N}_\mathrm{d} \subseteq \mathcal{N}_\mathrm{b}$, e.g., by comparing the received power level with a predefined threshold. The angle at which the beam pattern j points with the direction of the direct path as reference is denoted by θ_j. The AOA related to the centroid of the detected target is denoted by ϕ. The goal is to estimate ϕ based on the received power levels measured in the directions $\{\theta_j\colon j \in \mathcal{N}_\mathrm{d}\}$. In particular, the AOA estimate is obtained via a weighted average given by

$$\hat{\phi} = \frac{\sum_{j\in\mathcal{N}_\mathrm{d}} P_{\theta_j}\theta_j}{\sum_{j\in\mathcal{N}_\mathrm{d}} P_{\theta_j}}\,. \tag{3}$$

Note that the AOA estimates can be subject to biases caused by imprecise beam steering. Hence, we consider AOA estimates with and without the mitigation of such biases. Considering a constant bias, an unbiased estimator can be obtained by subtracting the mean of the biased estimator [30]. With the AOA estimation method in (3), the average absolute errors result to be 0.43° and 1.23° with and without bias mitigation, respectively. Moreover, the standard deviations of the absolute error with and without bias mitigation result to be 0.29° and 0.52°, respectively. This shows that the proposed technique can provide accurate AOA estimates in complex wireless environments.

The proposed method relies on measurements of the received power for N_d overlapping beam patterns detecting a target. This method is compatible with standardized 5G beam sweeping procedures providing such measurements. In particular, sensing with narrow beams can improve the estimation accuracy. While more sophisticated AOA estimation methods exist (e.g., see [20]), they are not fully compatible with standardized 5G systems and may require dedicated receivers or changes in the system architecture.

B. AOA Measurement Models

To explore 5G DFL at mm-Waves, we develop AOA measurement models based on experimental data. Such models are developed under the assumptions that the target is detected by adjacent and partially overlapping beam patterns and that the effects of the direct path and clutter are effectively mitigated.

The AOA measurement for a target with centroid in the direction ϕ can be modeled as

$$\breve{\varphi} = \phi + \varepsilon \tag{4}$$

with the random variable ε denoting the measurement error. The distribution of the measurement error is obtained by fitting its empirical distribution to a Gaussian mixture model (GMM) via the expectation maximization algorithm [31]. Let N_G and $\boldsymbol{\theta} = [\boldsymbol{w}^\mathrm{T}, \boldsymbol{\mu}^\mathrm{T}, \boldsymbol{\sigma}^\mathrm{T}]^\mathrm{T}$ denote the number of mixtures and the parameter vector with $\boldsymbol{w} = [w_1, w_2, \dots, w_{N_\mathrm{G}}]^\mathrm{T}$, $\boldsymbol{\mu} = [\mu_1, \mu_2, \dots, \mu_{N_\mathrm{G}}]^\mathrm{T}$, and $\boldsymbol{\sigma} = [\sigma_1, \sigma_2, \dots, \sigma_{N_\mathrm{G}}]^\mathrm{T}$. The GMM for ε with parameter vector $\boldsymbol{\theta}$ is given by

$$\breve{f}(\varepsilon;\boldsymbol{\theta}) = \sum_{i=1}^{N_\mathrm{G}} w_i\,\zeta(\varepsilon;\mu_i,\sigma_i^2) \tag{5}$$

with $\zeta(\varepsilon;\mu,\sigma^2)$ denoting the Gaussian distribution with mean μ and variance σ^2, and $w_i \in [0,1]$ such that $\sum_{i=1}^{N_\mathrm{G}} w_i = 1$.

To assess the quality of the models, we evaluate the Jensen-Shannon divergence (JSD) [31]. Let $\hat{f}(\varepsilon)$ and $\breve{f}(\varepsilon) = \breve{f}(\varepsilon;\boldsymbol{\theta})$ denote the empirical probability distribution function (PDF) of ε and its fitted model, respectively. The JSD is given by

$$D(\hat{f}\|\breve{f}) = \int \left[\frac{\hat{f}(\varepsilon)}{2}\log\left(\frac{\hat{f}(\varepsilon)}{g(\varepsilon)}\right) + \frac{\breve{f}(\varepsilon)}{2}\log\left(\frac{\breve{f}(\varepsilon)}{g(\varepsilon)}\right)\right] d\varepsilon \tag{6}$$

with $g(\varepsilon) = \left[\hat{f}(\varepsilon) + \breve{f}(\varepsilon)\right]/2$. A small value of the JSD indicates an accurate fit to the empirical distribution. Specifically, the JSD for GMMs considering $N_\mathrm{G} = 2$ with and without bias mitigation are 0.0057 and 0.0042, respectively, showing that the representations of the empirical distributions are accurate.

V. DFL Performance Based on 5G Experimentation

In this section, we explore 5G DFL at mm-Waves via simulations based on the developed AOA measurement models. Consider a multistatic DFL system consisting of a 5G BS emitting mm-Wave signals and four UEs as sensing receivers in an outdoor environment similar to that in the experimentation. We consider a single target placed randomly in the environment. The target position is estimated via least squares using AOA measurements obtained from the developed models. We evaluate the localization performance in terms of the empirical cumulative distribution function (ECDF) of the position error.

Fig. 4 shows the ECDF of the position error considering the AOA measurement models with and without bias mitigation. The ECDF indicates the probability that the position error is lower than or equal to the value in abscissa. Note that the performance is significantly improved by mitigating the

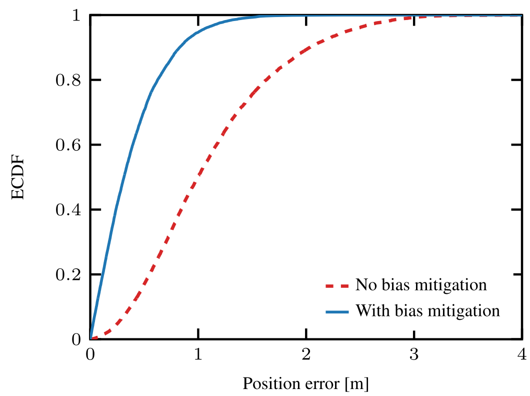

Fig. 4. 5G DFL performance at mm-Waves under AOA measurement models.

biases caused by imprecise beam steering. For example, the position errors are below 1.37 and 2.93 m for 99% of the cases considering the AOA measurement models with and without bias mitigation, respectively. These measurement-based results show the potential of 5G DFL at mm-Waves exploiting beam sweeping at the receiver. While the experimentation employs a probe signal, 5G DFL can exploit reference signals or reuse communication signals. These architectural aspects integrate seamlessly with existing procedures in 5G specifications [17]. In particular, extensive measurement campaigns and network experimentation [32] in diverse environments are required for the characterization and integration of DFL in 5G ecosystems.

VI. Final Remark

This letter presented an experimentation and measurement campaign for outdoor device-free target detection and localization using a 5G FWA at 28 GHz as transmitter. Specifically, we performed experiments to explore the sensing capabilities of 5G systems for providing DFL. Experimental results show the potential of 5G DFL at mm-Waves without modifying standardized signaling and baseband processing by exploiting beam sweeping procedures. In particular, the proposed AOA estimation technique based on the directions of overlapping beams detecting a target can achieve sub-degree accuracy in combination with precise beamforming. The experimental work in this letter paves the way for the characterization and integration of DFL at mm-Waves in 5G and B5G ecosystems.

References

[1] *Technical Specification Group Radio Access Network; Study on NR Positioning Support*, 3GPP, document TR 38.855, Mar. 2019.

[2] A. Conti et al., "Location awareness in beyond 5G networks," *IEEE Commun. Mag.*, vol. 59, no. 11, pp. 22–27, Nov. 2021.

[3] *Technical Specification Group TSG SA; Feasibility Study on Integrated Sensing and Communication*, 3GPP, document TR 22.837, Mar. 2023.

[4] M. Z. Win et al., "Network localization and navigation via cooperation," *IEEE Commun. Mag.*, vol. 49, no. 5, pp. 56–62, May 2011.

[5] F. Liu et al., "Integrated sensing and communications: Toward dual-functional wireless networks for 6G and beyond," *IEEE J. Sel. Areas Commun.*, vol. 40, no. 6, pp. 1728–1767, Jun. 2022.

[6] M. I. Skolnik, *Radar Handbook*, 3rd ed. New York, NY, USA: Mcgraw-Hill, 2008.

[7] M. Chiani, A. Giorgetti, and E. Paolini, "Sensor radar for object tracking," *Proc. IEEE*, vol. 106, no. 6, pp. 1022–1041, Jun. 2018.

[8] S. Bartoletti, Z. Liu, M. Z. Win, and A. Conti, "Device-free localization of multiple targets in cluttered environments," *IEEE Trans. Aerosp. Electron. Syst.*, vol. 58, no. 5, pp. 3906–3923, Oct. 2022.

[9] Samsung Electronics, *5G Fixed Wireless Access*. Gyeonggi-Do, South Korea: Samsung Electronics Co., Ltd., 2018.

[10] P. Falcone, F. Colone, and P. Lombardo, "Potentialities and challenges of WiFi-based passive radar," *IEEE Aerosp. Electron. Syst. Mag.*, vol. 27, no. 11, pp. 15–26, Nov. 2012.

[11] F. Colone, P. Falcone, C. Bongioanni, and P. Lombardo, "WiFi-based passive bistatic radar: Data processing schemes and experimental results," *IEEE Trans. Aerosp. Electron. Syst.*, vol. 48, no. 2, pp. 1061–1079, Apr. 2012.

[12] P. Stinco, M. S. Greco, F. Gini, and B. Himed, "IEEE 802.22 passive radars: Multistatic detection and velocity profiler," *IEEE Trans. Aerosp. Electron. Syst.*, vol. 52, no. 5, pp. 2298–2313, Oct. 2016.

[13] *Technical Specification Group Radio Access Network; NR; Base Station (BS) Radio Transmission and Reception*, 3GPP, document TS 38.104, Jun. 2022.

[14] M. Z. Win, Y. Shen, and W. Dai, "A theoretical foundation of network localization and navigation," *Proc. IEEE*, vol. 106, no. 7, pp. 1136–1165, Jul. 2018.

[15] A. Shastri et al., "A review of millimeter wave device-based localization and device-free sensing technologies and applications," *IEEE Commun. Surveys Tuts.*, vol. 24, no. 3, pp. 1708–1749, 3rd Quart., 2022.

[16] M. Giordani, M. Polese, A. Roy, D. Castor, and M. Zorzi, "A tutorial on beam management for 3GPP NR at mmWave frequencies," *IEEE Commun. Surveys Tuts.*, vol. 21, no. 1, pp. 173–196, 1st Quart., 2019.

[17] *Technical Specification Group Radio Access Network; Study on New Radio Access Technology Physical Layer Aspects*, 3GPP, document TR 38.802, Sep. 2017, Release 14.

[18] J. A. Zhang et al., "An overview of signal processing techniques for joint communication and radar sensing," *IEEE J. Sel. Topics Signal Process.*, vol. 15, no. 6, pp. 1295–1315, Nov. 2021.

[19] G. Kwon, A. Conti, H. Park, and M. Z. Win, "Joint communication and localization in millimeter wave networks," *IEEE J. Sel. Topics Signal Process.*, vol. 15, no. 6, pp. 1439–1454, Nov. 2021.

[20] L. Pucci, E. Paolini, and A. Giorgetti, "System-level analysis of joint sensing and communication based on 5G New Radio," *IEEE J. Sel. Areas Commun.*, vol. 40, no. 7, pp. 2043–2055, Jul. 2022.

[21] R. S. Thoma et al., "Cooperative passive coherent location: A promising 5G service to support road safety," *IEEE Commun. Mag.*, vol. 57, no. 9, pp. 86–92, Sep. 2019.

[22] P. Samczynski et al., "5G network-based passive radar," *IEEE Trans. Geosci. Remote Sens.*, vol. 60, 2022, Art. no. 5108209.

[23] O. Kanhere, S. Goyal, M. Beluri, and T. S. Rappaport, "Target localization using bistatic and multistatic radar with 5G NR waveform," in *Proc. IEEE 93rd Veh. Technol. Conf.*, Helsinki, Finland, Apr. 2021, pp. 1–7.

[24] J. Ko et al., "Millimeter-wave channel measurements and analysis for statistical spatial channel model in in-building and urban environments at 28 GHz," *IEEE Trans. Wireless Commun.*, vol. 16, no. 9, pp. 5853–5868, Sep. 2017.

[25] Y. Xing and T. S. Rappaport, "Millimeter wave and terahertz urban microcell propagation measurements and models," *IEEE Commun. Lett.*, vol. 25, no. 12, pp. 3755–3759, Dec. 2021.

[26] J. Du et al., "Directional measurements in urban street canyons from macro rooftop sites at 28 GHz for 90% outdoor coverage," *IEEE Trans. Antennas Propag.*, vol. 69, no. 6, pp. 3459–3469, Jun. 2021.

[27] X. Li, X. Wang, Q. Yang, and S. Fu, "Signal processing for TDM MIMO FMCW millimeter-wave radar sensors," *IEEE Access*, vol. 9, pp. 167959–167971, 2021.

[28] *Air Interface Working Group; Verizon 5th Generation Radio Access; Physical Channels and Modulation*, Verizon 5G TF, document TS V5G.211, Jun. 2016.

[29] K. J. Sangston, F. Gini, and M. S. Greco, "Coherent radar target detection in heavy-tailed compound-Gaussian clutter," *IEEE Trans. Aerosp. Electron. Syst.*, vol. 48, no. 1, pp. 64–77, Jan. 2012.

[30] H. L. Van Trees, *Detection, Estimation, and Modulation Theory*, 1st ed. New York, NY, USA: Wiley, 1968.

[31] K. P. Murphy, *Machine Learning: A Probabilistic Perspective*. Cambridge, MA, USA: MIT Press, 2012.

[32] A. Conti, M. Guerra, D. Dardari, N. Decarli, and M. Z. Win, "Network experimentation for cooperative localization," *IEEE J. Sel. Areas Commun.*, vol. 30, no. 2, pp. 467–475, Feb. 2012.

Open Access funding provided by 'Università degli Studi di Ferrara' within the CRUI CARE Agreement